Publishing Excellence
Inspiring Progress

ISSN: 3143-0732 https://aristonpubs.com/journal/science-of-alloys-and-glasses https://doi.org/10.69626/sag.2025.0028

RESEARCH ARTICLE

Radiation Shielding Performance of Dense Tellurite Glasses Doped with Rare Earth Oxides against High–Energy Photons and Neutrons

Zahrah S.A Almutawah [1], Ibrahim Hadadi [2], Awad Almarhaby [3], Ibtesam S. Asiri [1], Elhussaien Elshiekh[2], Badriah Sultan [1, *]

ABSTRACT: This research presents an experimental investigation into the radiation shielding capabilities of newly developed tellurite-based glasses incorporating rare earth oxides. The glass systems were synthesized with a base composition of $45TeO_2$–$25B_2O_3$–$20Bi_2O_3$–$7TiO_2$–3RE, where RE represents La_2O_3, Ce_2O_3, Sm_2O_3, Er_2O_3, and Yb_2O_3. The attenuation behavior of these glasses was assessed using gamma-ray spectroscopy across a range of energies (59.5 keV to 1330 keV) derived from Am-241, Cs-137, and Co-60 radioactive sources. Fundamental shielding parameters such as linear and mass attenuation coefficients, half-value layer, tenth-value layer, mean free path, effective atomic number, and fast neutron removal cross-section were determined experimentally. These findings were further validated and extended across a broader energy spectrum (0.015–15 MeV) using the Phy-X/PSD simulation software. Results indicate that all fabricated glasses offer considerable photon attenuation, with performance directly linked to material density. The Yb-doped variant (BBTTYb) achieved the highest density of 6.31 g/cm³ and demonstrated the most effective shielding properties, including the lowest half-value layer and mean free path across the majority of energy levels. The improved attenuation is credited to the rise in effective atomic number and electron density resulting from the inclusion of heavy rare earth elements. This study confirms that doping tellurite glasses with rare earth oxides, especially Yb_2O_3, markedly enhances their gamma-ray shielding efficiency. These advanced glass systems hold significant promise for deployment in medical, industrial, and research settings that require robust radiation protection over a wide energy range.

Keywords: Radiation shielding, Tellurite glass, Rare-earth oxides, Attenuation coefficients, Neutron shielding, Protective materials.

Received: 11 October 2024; Revised: 14 November 2024; Accepted: 21 December 2024; Published Online: 30 January 2025

1. INTRODUCTION

Radiation protection remains a critical pillar in safeguarding human health within environments where ionizing radiation is utilized, such as medical diagnostics, radiotherapy, nuclear power generation, and scientific research. The primary objective is to prevent deterministic biological effects, which have a threshold dose, and to minimize the probability of stochastic effects, such as cancer, which can occur at any exposure level [1]. This imperative is operationalized through the "as low as reasonably achievable" (ALARA) principle, a cornerstone of radiological safety that mandates the optimization of protective measures. While reducing exposure time and maximizing distance from the radiation source are fundamental strategies, the incorporation of effective shielding materials between the source and personnel is often the most robust and practical line of

[1] Department of Physics, Faculty of Science, King Khalid University, AlQuraa, Abha, P. O. Box 906, Saudi Arabia..
[2] Department of Radiological Sciences, College of Applied Medical Sciences, King Khalid University, AlQuraa, Abha, P. O. Box 906, Saudi Arabia.
[3] Medical Physics Department, King Fahd General Hospital, Ministry of Health, Al Andalus, Jeddah 23325, Jeddah, Saudi Arabia.

* Author to whom correspondence should be addressed: bsoltan@kku.edu.sa (Badriah Sultan)

© Ariston Publications 2025. All rights reserved.

defense [2]. For decades, lead (Pb) and lead-based composites, including lead glass, have been the traditional materials of choice for this purpose due to their high atomic number and density, which confer excellent attenuation properties against X-rays and gamma rays. However, the significant toxicity of lead poses severe environmental and health hazards, ranging from soil and groundwater contamination to neurological damage in humans, complicating its lifecycle from manufacturing to disposal. Furthermore, lead glass suffers from inherent material weaknesses, including brittleness, opacity to visible light in some formulations, and poor mechanical durability, which limit its application in settings requiring transparency or structural resilience [3]. Consequently, the global scientific community has been actively pursuing the development of novel, high-performance, and environmentally benign shielding materials that can match or surpass lead's protective capabilities without its associated drawbacks.

Among the various candidate systems, tellurite-based glasses (TeO_2) have emerged as a particularly promising host matrix for advanced radiation shielding applications. Tellurite glasses are not a new discovery; their unique properties have been exploited for years in diverse technological fields including thermoelectric devices, optical fiber amplifiers, laser hosts, and gas sensing apparatus [4-9]. Their attractiveness stems from a favorable combination of physical and chemical attributes: they exhibit good infrared transparency, relatively high linear and nonlinear refractive indices, satisfactory thermal stability, a relatively low melting point compared to silicate glasses, and notable corrosion resistance, all achievable in a cost-effective manufacturing process [10–14]. These characteristics make them versatile for integration into complex systems. However, pure TeO_2 glass has a structural limitation due to relatively weak Te–O bonds, which can constrain its network-forming ability and mechanical strength. To engineer a stable and functionally enhanced glass matrix, the incorporation of modifiers is essential.

The addition of heavy metal oxides (HMOs) or rare earth (RE) ions serves a dual purpose: it stabilizes the glass network and dramatically improves its radiation interaction cross-section. When tellurium oxide is combined with high-Z modifiers like bismuth oxide (Bi_2O_3), titanium dioxide (TiO_2), or lanthanum oxide (La_2O_3), the resulting composite exhibits significantly enhanced density and effective atomic number. This directly translates to superior shielding capabilities, extending the potential use of these glasses into demanding applications such as radiotherapy bunkers, nuclear medicine suites, industrial radiography, and particle accelerator facilities [15]. The enhanced performance is attributed to the increased probability of photon interactions, photoelectric absorption, Compton scattering, and pair production, driven by the elevated electron density provided by the heavy constituent atoms.

Bismuth oxide, in particular, has been identified as an exceptionally effective glass former and modifier. It is frequently employed as a non-toxic replacement for hazardous heavy metals like lead and cadmium in glass formulations. Bi_2O^3 introduces high density and polarizability into the glass network, which not only improves radiation attenuation but also can enhance the glass's resistance to thermal shock, a valuable property for applications involving thermal cycling [16]. Its melting temperature is compatible with tellurite-based systems, facilitating the synthesis of homogeneous, dense glasses suitable for shielding purposes [17].

The scientific literature reflects sustained interest in optimizing tellurite glass compositions for shielding. For instance, Udovic et al. investigated the structural and thermal characteristics of glasses within the Bi_2O_3–TiO_2–TeO_2 system, finding that the addition of TiO_2 and Bi_2O_3 modifiers increased the thermal stability of the glass, a crucial factor for practical deployment [18]. Halimah et al. demonstrated a direct correlation between increasing Bi_2O_3 content, elevated sample density, and improved gamma-ray shielding effectiveness in boro-tellurite glasses [19]. Research by Susoy on a Li_2O–B_2O_3–P_2O_5–TeO_2 system confirmed that the inclusion of TeO_2 significantly boosts nuclear radiation shielding efficiency [3]. Further studies have explored the role of other modifiers. Albarzan et al. experimentally showed that in a Na_2O–CaO–SiO_2–TiO_2 glass system, the highest linear attenuation coefficient (LAC) across a broad energy spectrum (0.015–15 MeV) was achieved with the sample containing the maximum concentration of TiO_2 (9 mol%) [20]. Elkhoshkhany et al. examined a multi-component system (B_2O_3, Bi_2O_3, TeO_2, TiO_2) doped with La_2O_3, reporting promising optical and gamma attenuation properties, suggesting suitability for dual-purpose optical and shielding windows [21]. Hussein et al. focused on a $70TeO_2$–$5Ta_2O_5$–$20Bi_2O_3$ composition, reporting a radiation protection efficiency (PRE) between 99.9% and 83.9% for low-energy photons (15–200 keV) and a rising LAC with increasing Bi_2O_3 concentration [22]. Collectively, these studies underscore the potential of tellurite glasses but also highlight the ongoing quest for optimal compositions that balance superior attenuation across a wide energy range with practical material properties.

The novelty of the present work lies in its focused investigation of a specific, dense glass series within the TeO_2–Bi_2O_3–TiO_2–La_2O_3 quaternary system, designed to systematically evaluate the synergistic effects of incremental lanthanum oxide doping on both photon and neutron attenuation. While previous studies have often examined individual modifiers or broader compositional ranges, this research provides a detailed, comparative analysis of how controlled substitution of TiO_2 with La_2O_3 influences key shielding parameters. The objective of this paper is to comprehensively investigate the radiation shielding capabilities of these novel glass systems, specifically within a critical low-to-intermediate photon energy range of 0.015 to 0.15 MeV, which is highly relevant for numerous medical and industrial isotopes. Utilizing the established Phy-X/PSD simulation software [23], a suite of essential radiation shielding parameters will be calculated and analyzed, including the mass attenuation coefficient (MAC), linear attenuation coefficient (LAC), half-value layer (HVL), tenth-

© Ariston Publications 2025. All rights reserved.

value layer (TVL), mean free path (MFP), effective atomic number (Z_{eff}), and effective electron density (N_{eff}). Furthermore, recognizing the importance of mixed radiation fields, this study extends its evaluation to include the fast neutron removal cross-section (FNRCS) to assess the material's potential for neutron shielding. The performance of these newly fabricated tellurite glasses will be benchmarked against commercially available standard shielding materials to critically appraise their practical viability and potential to serve as effective, non-toxic alternatives in next-generation radiation protection applications.

2. EXPERIMENTAL DETAILS

2.1. Glass Synthesis and Characterization

A series of tellurite-based glasses with the nominal composition $65TeO_2–25Bi_2O_3–(10\text{-}x)TiO_2–xLa_2O_3$, where x = 1, 2, 3, and 4, was designed and synthesized. This compositional matrix, designated as the TBTL series, was formulated to systematically investigate the role of lanthanum oxide (La_2O_3) as a substituting modifier for titanium dioxide (TiO_2) while maintaining a constant high content of the heavy glass-former bismuth oxide (Bi_2O_3). High-purity (≥ 99%) raw chemical powders of tellurium(IV) oxide (TeO_2), bismuth(III) oxide (Bi_2O_3), titanium(IV) oxide (TiO_2), and lanthanum(III) oxide (La_2O_3), all sourced from Sigma-Aldrich, were used as starting materials. Precise batches of 20 grams total weight were calculated based on molar percentages, meticulously weighed using an analytical balance with a precision of ±0.0001 g, and homogenized in an agate mortar to ensure a uniform mixture prior to melting.

The mixed batches were transferred to a high-purity platinum crucible to prevent contamination during the high-temperature process. Melting was conducted in an electrically heated furnace at a temperature of 950 °C, held for a duration of 30 minutes. Throughout the melting period, the melt was stirred periodically using a platinum rod to promote chemical homogeneity and to eliminate air bubbles. The resultant homogeneous, viscous melt was subsequently cast into a preheated graphite mold to form disc-shaped samples. To mitigate internal mechanical stresses induced by rapid cooling, the as-cast glasses were immediately transferred to a separate annealing furnace and subjected to a controlled thermal treatment. This annealing process was performed at a temperature of 300 °C for 2 hours, after which the furnace was switched off to allow the samples to cool gradually to ambient temperature within the chamber. The obtained glass samples were then ground and polished to achieve parallel, optically flat surfaces suitable for density measurement and subsequent radiation attenuation studies.

The physical density (ρ) of each prepared glass sample, a critical parameter directly influencing shielding performance, was determined using a helium gas pycnometer (UltraPyc 1200e, Quantachrome Instruments). This technique, based on gas displacement, provides highly accurate and reproducible density values. The measurement was performed at room temperature, and the reported density for each composition represents the average of five consecutive readings, with the instrument's specified accuracy being 0.0003%. The measured densities, alongside the corresponding sample codes and nominal compositions in mole percent, are compiled in Table 1.

Table 1. Sample codes, nominal chemical compositions in mole fraction (%), and measured densities of the synthesized TBTL glass systems.

Density (g/cm³)	TeO_2	Bi_2O_3	TiO_2	La_2O_3	Sample Code
6.4400	65	25	10	0	TBT
6.4541	65	25	9	1	TBTL1
6.4670	65	25	8	2	TBTL2
6.4821	65	25	7	3	TBTL3
6.5121	65	25	6	4	TBTL4

2.2. Theoretical Framework for Shielding Evaluation

The assessment of a material's efficacy for radiation shielding necessitates the calculation of several fundamental parameters, which describe the statistical nature of photon and neutron interactions with matter. The primary quantity is the linear attenuation coefficient (μ, in cm^{-1}), defined for a narrow, collimated beam of monoenergetic photons. It describes the fractional decrease in beam intensity (I) per unit thickness (x) of the absorber material and is derived from the Beer-Lambert law:

$$I = I_0 e^{-\mu x} \quad (1)$$

Where I, denotes the attenuated intensity of the photon beam in the interaction media and I_0, the unattenuated intensity of the photon beam. Consequently, μ can be expressed as:

$$\mu = \mathrm{LAC} = -\frac{\ln\frac{I}{I_0}}{x} \quad (2)$$

The mass attenuation coefficient MAC is physical quantities that measure the permeation of ionizing radiation through a material. The MAC can be calculated using the following equation [24, 25]:

$$\mathrm{MAC} = \mu m = \frac{\mu}{\rho} = \sum wi \left(\frac{\mu}{\rho}\right)_i \quad (3)$$

Where w_i indicates the fractional weight and $\left(\frac{\mu}{\rho}\right)_i$ the MAC of the individual component of each element, and ρ the density of the attenuated material.

Half-value attenuation of ionizing photons (HVL) is an important radiation shielding properties that can be used to provide accurate measurements of the required shielding

© Ariston Publications 2025. All rights reserved.

thickness. The HVL are calculated by the following equation [25]:

$$\mathrm{HVL} = \frac{0.693}{\mathrm{LAC}} \quad (4)$$

Tenth-value layers TVLs represent the thickness of matter that minimize incoming radiation by tenth of its intensity. The TVLs are calculated by following equation [26]:

$$\mathrm{TVL} = \frac{2.3}{\mathrm{LAC}} \quad (5)$$

A single particle's mean free path (MFP) shows the average distance traveled before they interact with the material. MFP is extremely important in determining radiation shielding performance. The MFP are calculated by following equation [25]:

$$\mathrm{MFP} = \frac{1}{\mathrm{LAC}} \quad (6)$$

An effective electron density N_{eff} and effective atomic number Z_{eff} are important factors in radiation shielding materials. The Z_{eff} are calculated by following equation [25]:

$$Z_{eff} = \frac{\sum_i f_i A_i \left(\frac{\mu}{\rho}\right)_i}{\sum_j f_j \frac{A_j}{z_j} \left(\frac{\mu}{\rho}\right)_j} \quad (7)$$

Where, f_i is the ith atomic element of the mole fraction, A_i is the atomic weight of the ith atomic element, and Z_j is the atomic number.

N_{eff} is the number of electrons in each unit mass, a strong relationship exists between N_{eff} and Z_{eff}, which is calculated by following equation [25]:

$$N_{eff} = \frac{(\mu/\rho)}{\sigma_t} = \frac{N_A}{M} Z_{eff} \sum_i n_i = \frac{N_A Z_{eff}}{A} \quad (8)$$

Where, N_A, M and $\sum_i n_i$ are the Avogadro number, the molecular weight and the total number of compound elements in the radiation shielding materials, respectively.

The integrated atomic and electronic cross-section values of the photons ACS, ECS can be used to define how incoming photons could interfere with the atoms and electrons of the composite materials. ACS and ECS are calculated by following equations [24]:

$$\mathrm{ACS} = \sigma_T = \left[\frac{1}{N_A}\right] \sum_i f_i A_i \left(\frac{\mu}{\rho}\right) = \frac{\sigma_{t,m}}{\sum_i n_i} \quad (9)$$

$$ECS = \sigma_e = \left[\frac{1}{N_A}\right] \sum_i \frac{f_i A_i}{Z_I} \left(\frac{\mu}{\rho}\right)_i = \frac{\sigma_{t,a}}{Z_{eff}} \quad (10)$$

To determine the ability of specific shielding materials to harden neutrons, the fast neutron-removal cross-section (FNRCS) is calculated with the following equation [27]:

$$\Sigma_R = \sum_i \rho_i (\Sigma_R/\rho) \quad (11)$$

Where ρ_i and $(\Sigma R/\rho)_i$ represent the partial density.

In this study, all the aforementioned shielding parameters for the synthesized TBTL glasses were calculated computationally over a broad energy spectrum using the well-established Phy-X/PSD software tool [23].

3. RESULTS AND DISCUSSION

3.1. Photon Attenuation Coefficients

The radiation shielding characteristics of the synthesized TBTL glass series, alongside the base TBT composition and several commercial shielding glasses, were evaluated computationally across an extensive photon energy spectrum from 0.015 to 15 MeV. The fundamental parameters describing a material's innate ability to attenuate photons are the mass attenuation coefficient (MAC) and the linear attenuation coefficient (LAC). Figure 1(a) illustrates the variation of MAC with energy for all prepared glasses. A consistent trend is observed across all samples: the MAC values are highest at the lowest energies and undergo a steep, exponential decline as energy increases up to approximately 100 keV. This is followed by a more gradual decrease throughout the intermediate energy region. Figure 1(b) presents the corresponding LAC, which follows a qualitatively similar trend but its magnitude is directly scaled by the sample density (ρ), as per the relation LAC = MAC × ρ. Consequently, the sample with the highest density (TBTL4) consistently exhibits the greatest LAC across nearly the entire energy range, confirming that increased density directly enhances photon stopping power [28].

The energy dependence of these coefficients is governed by the dominant photon interaction mechanisms. The very high values at energies below 0.1 MeV are attributable to the photoelectric effect, the cross-section for which is proportional to approximately Z^4/E^3, where Z is the effective atomic number and E is the photon energy [28]. The prominent peak observed near 0.1 MeV for all samples corresponds to the K-absorption edge of bismuth (Bi, Z=83), a major constituent, which causes a sharp increase in the photoelectric absorption cross-section. As energy increases into the 0.1 to 5 MeV range, Compton scattering becomes the predominant interaction. Its cross-section per electron is roughly independent of atomic number and decreases slowly with increasing energy, leading to the observed gradual decline in both MAC and LAC [28]. For energies exceeding 6 MeV, the onset of pair production, with a cross-section proportional to Z^2, contributes to the slight gradual increase observed in the coefficients at the highest energies studied [29]. Critically, the TBTL4 sample (4 mol% La_2O_3, density 6.5121 g/cm³) demonstrated the best overall shielding performance, exhibiting the highest MAC and LAC values among the prepared series at any given energy, particularly in the critical therapeutic and industrial energy ranges.

To contextualize the performance of these novel materials, their LAC was benchmarked against three commercially available radiation shielding glasses: RS-253

© Ariston Publications 2025. All rights reserved.

G18, RS-360, and RS-520 [30]. As shown in Figures 1(c) and 1(d), which compare LAC at two high energies relevant to radiotherapy (6 MeV and 10 MeV), the prepared TBTL glasses significantly outperform the commercial standards. For instance, at 6 MeV, the LAC of TBTL4 is more than double that of RS-360 and triple that of RS-253 G18. This superior attenuation at high energies underscores the potential of these dense tellurite glasses for applications in high-energy photon environments, such as radiation therapy linear accelerator bunkers and industrial radiography facilities, where minimizing shield thickness is a paramount engineering concern.

3.2. Half-Value Layer and Mean Free Path

The half-value layer (HVL) and mean free path (MFP) are derived, practical parameters that directly inform the required thickness of a shielding material. Figure 2(a) displays the HVL for the investigated glasses as a function of energy. As anticipated from the inverse relationship with LAC (HVL = 0.693/μ), the HVL is lowest at minimal energies and increases with photon energy, plateauing at higher energies where the LAC becomes relatively constant. A lower HVL indicates that a thinner slab of material is sufficient to halve the radiation intensity, which is highly desirable. Among the prepared glasses, TBTL4 consistently possesses the smallest HVL across the spectrum, meaning it requires the least material to achieve the same level of attenuation. The MFP, representing the average distance between photon interactions (MFP = 1/μ), shows an identical energy-dependent trend, as depicted in Figure 2(b). A shorter MFP signifies a higher probability of interaction per unit distance traveled, further confirming the superior shielding density of the La_2O_3-enriched compositions.

The comparative advantage of the TBTL glasses is starkly evident in Figures 2(c) and 2(d), which present HVL and MFP values at 6 MeV, respectively. The numerical HVL values at this energy were 2.848, 2.841, 2.835, 2.828, and 2.814 cm for TBT, TBTL1, TBTL2, TBTL3, and TBTL4, in that order. This progression shows a clear, albeit small, improvement with each incremental addition of La_2O_3.

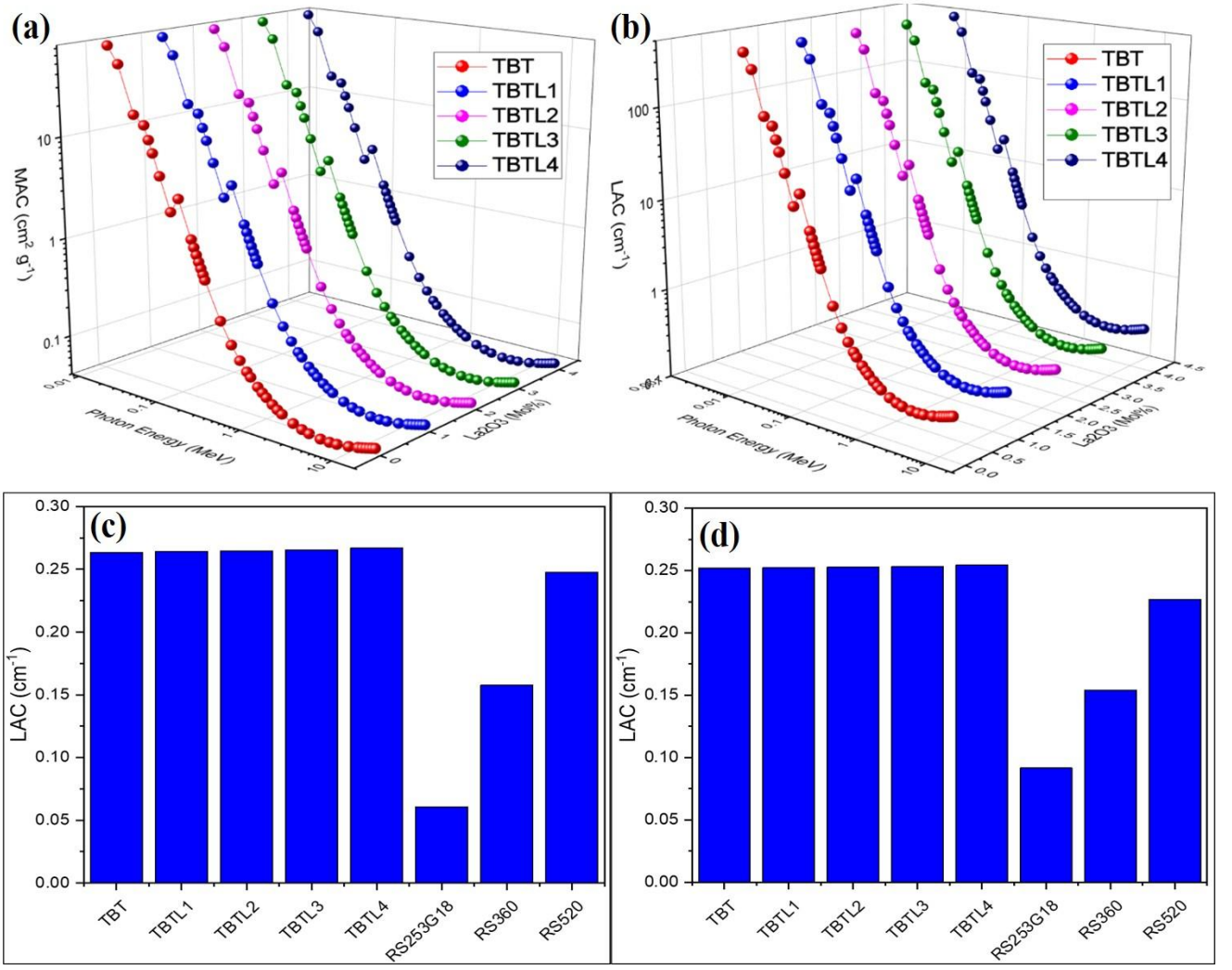


Fig. 1. (a) Mass attenuation coefficient (MAC) and (b) Linear attenuation coefficient (LAC) as a function of photon energy (0.015–15 MeV) for the prepared TBTL glass series. Comparison of LAC values between the prepared glasses and commercial shielding materials at (c) 6 MeV and (d) 10 MeV photon energy.

© Ariston Publications 2025. All rights reserved.

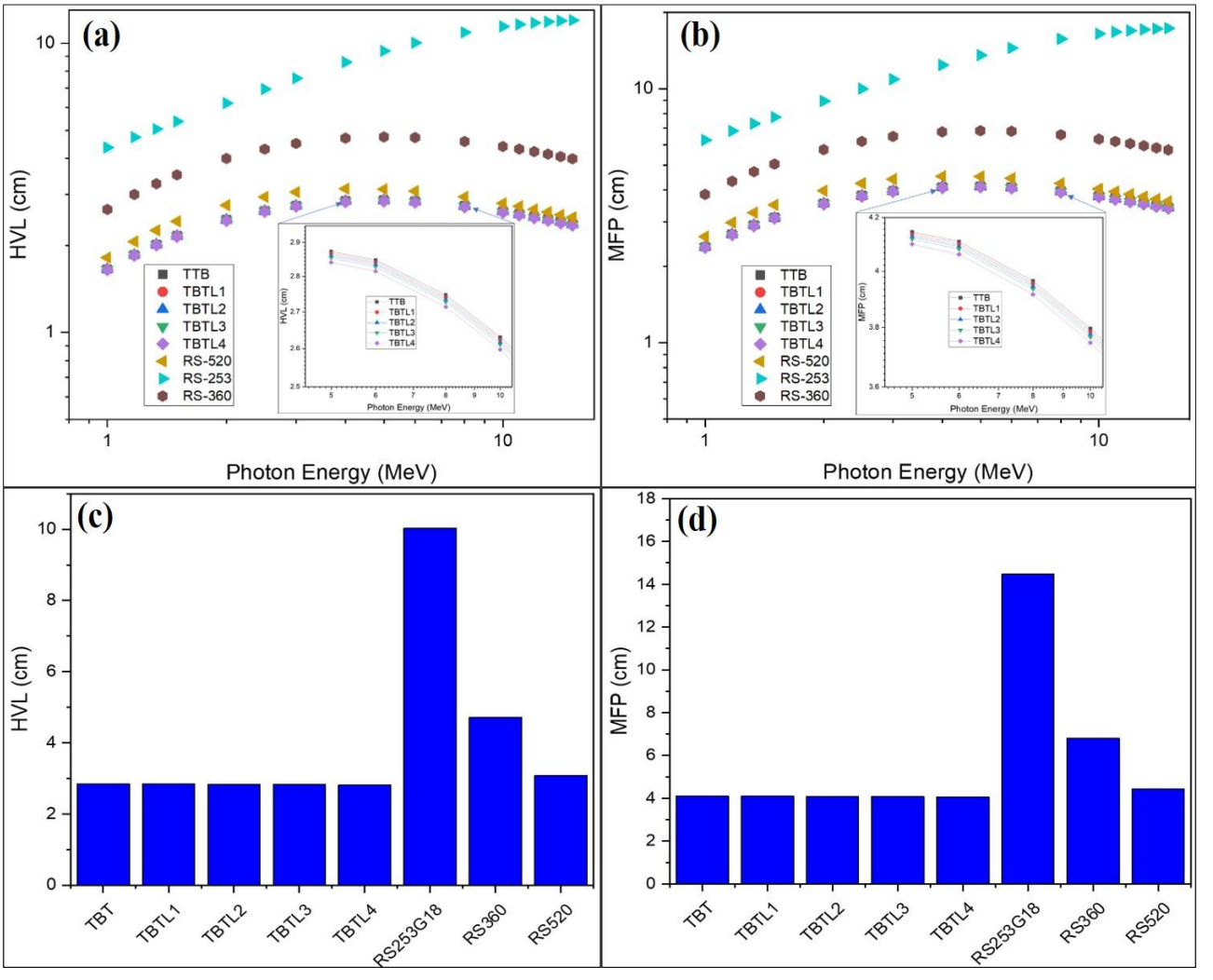


Fig. 2. (a) Half-value layer (HVL) and (b) Mean free path (MFP) for the TBTL glass series over the energy range 0.015–15 MeV. Comparative bar charts of (c) HVL and (d) MFP for all investigated materials at a photon energy of 6 MeV.

In contrast, the commercial glasses RS-253 G18, RS-360, and RS-520 exhibited significantly larger HVLs of 10.03, 4.72, and 3.08 cm, respectively. The HVL of the best-performing TBTL4 glass is approximately 27% lower than that of the closest commercial competitor (RS-520) at this energy. This translates directly into the potential for more compact, lighter, or more effective shielding structures when using the developed tellurite glasses.

3.3. Effective Atomic Number and Electron Density

The effective atomic number (Z_{eff}) and effective electron density (N_{eff}) are composite parameters that provide a deeper understanding of the photon interaction behavior of a multi-element material. Figure 3(a) shows the energy dependence of Z_{eff} for the TBT and TBTL4 samples, which represent the boundaries of the studied composition range. Both samples exhibit a very high Z_{eff} at the lowest energy (0.015 MeV), which plunges sharply to a minimum around 0.1 MeV before gradually increasing again at energies above 10 MeV. This complex behavior is a direct signature of the shifting dominance between interaction processes [14]. The initial sharp drop is characteristic of the photoelectric effect, where the cross-section's strong Z-dependence makes the effective Z appear very high. The minimum and plateau region through the Compton dominance zone reflects the fact that Compton scattering cross-section is largely independent of Z. The gradual rise at high energies is due to the growing contribution of pair production, a process with a Z^2 dependence.

N_{eff}, plotted in Figure 3(b), displays a nearly identical trend, as it is intrinsically linked to Z_{eff} through the material's molecular composition. The fact that TBTL4 maintains marginally higher Z_{eff} and N_{eff} values than TBT across most of the energy spectrum, particularly in the photoelectric and pair production regions, reinforces the role of La (Z=57) in enhancing the overall electron density and photon interaction probability compared to the base composition containing only Ti (Z=22). This provides a fundamental, atomic-level explanation for the observed improvements in MAC, LAC, HVL, and MFP with increasing La_2O_3 content.

© Ariston Publications 2025. All rights reserved.

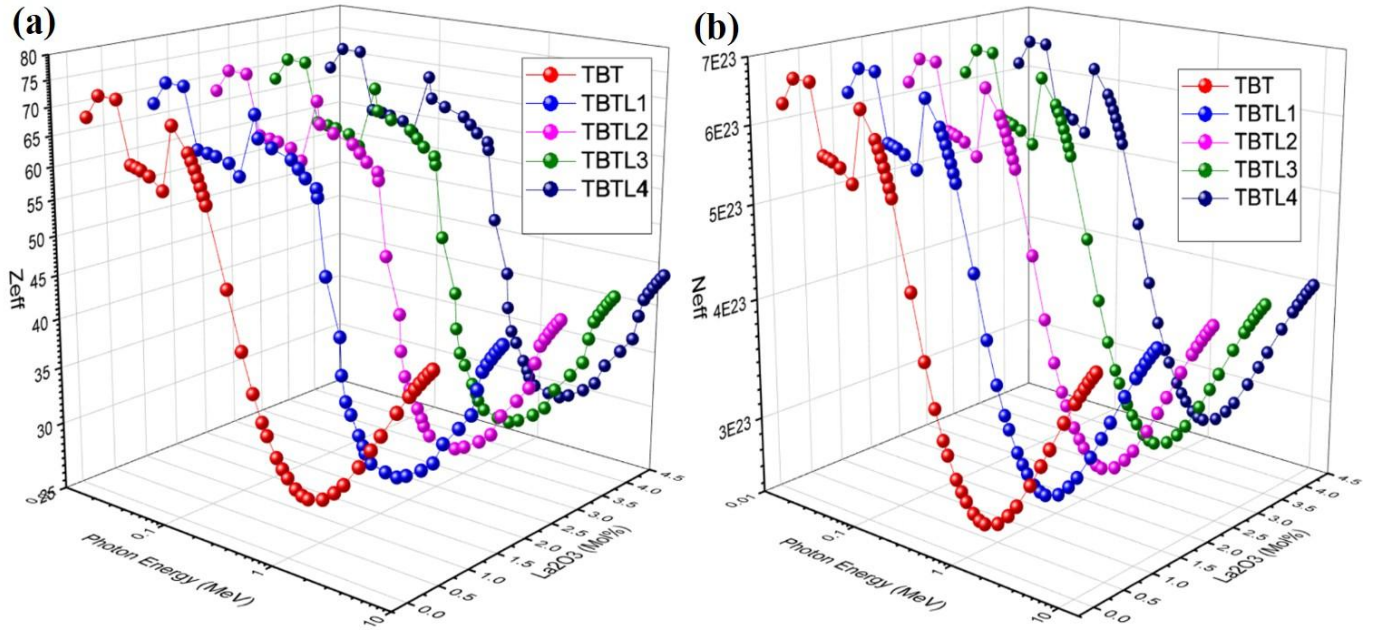


Fig. 3. Variation of (a) effective atomic number (Z_{eff}) and (b) effective electron density (N_{eff}) with photon energy for the base TBT and the highest-density TBTL4 glass samples.

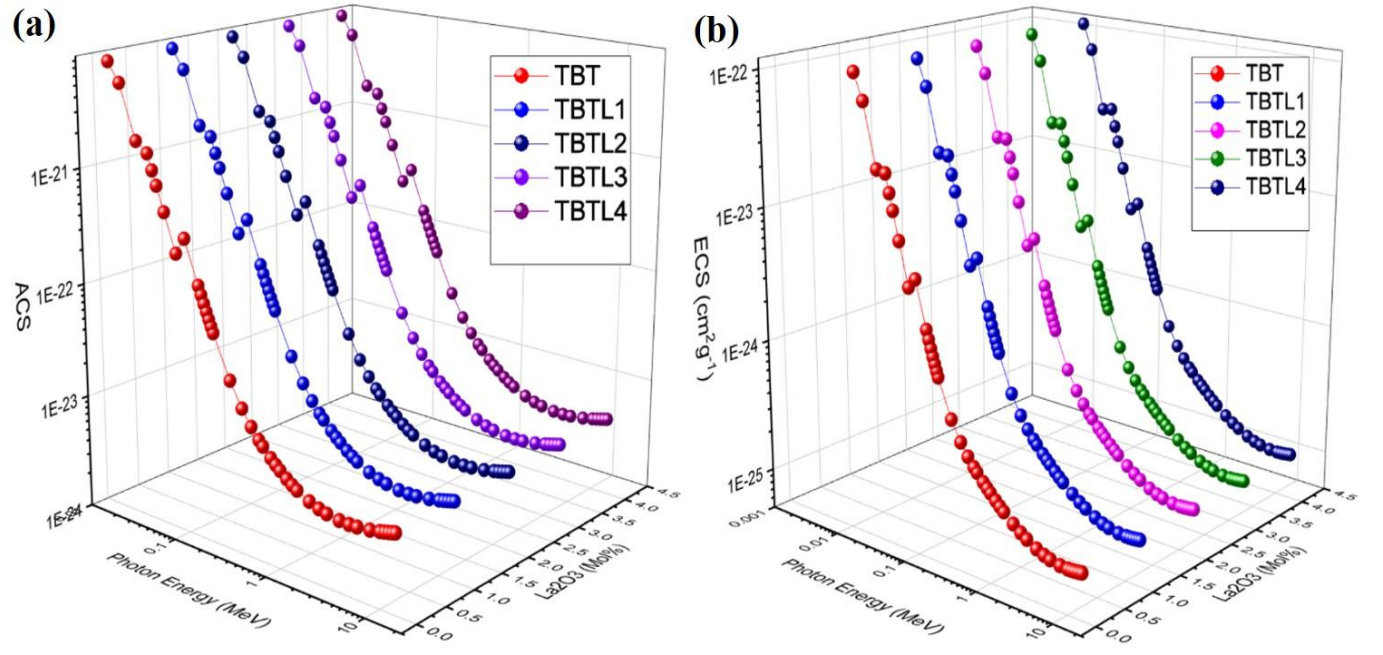


Fig. 4. (a) Atomic cross-section (ACS) and (b) Electronic cross-section (ECS) as functions of photon energy for the prepared TBTL glass systems.

3.4. Atomic and Electronic Cross-Sections

To further dissect the interaction mechanics, the atomic cross-section (ACS) and electronic cross-section (ECS) were calculated. The ACS, shown in Figure 4(a), represents the probability of interaction per atom, while the ECS (Figure 4(b)) represents the probability per electron. The energy profiles of both parameters mirror those of Z_{eff} and N_{eff}, for which they serve as foundational calculations. Higher ACS and ECS values are desirable as they indicate a greater chance of an incident photon interacting with an individual atom or electron within the shielding medium. The graphs demonstrate that all glasses in the series follow the same pattern, with TBTL4 generally yielding the highest cross-section values. This confirms that the improvement in shielding is not merely a function of increased mass density

 © Ariston Publications 2025. All rights reserved.

but is also due to a more favorable interaction cross-section at the atomic level, stemming from the modified chemical composition. The close overlap of the curves for different TBTL compositions indicates that while the substitution of La for Ti brings measurable benefits, the core interaction physics within this specific chemical family remains consistent.

3.5. Neutron Shielding Potential

While optimized for photon attenuation, the potential of the TBTL glasses for neutron shielding was assessed via the fast neutron removal cross-section (Σ_R). Figure 5 presents a bar chart comparing the calculated Σ_R values for the TBTL glasses with those of the same commercial standards. The results indicate that the Σ_R for the TBTL series is relatively consistent, ranging between approximately 0.105 and 0.108 cm^{-1}, showing no significant variation with La_2O_3 concentration. This is expected because neutron interaction depends primarily on nuclear composition and density, and the substitution of La for Ti does not drastically alter the light element content, such as oxygen, which is crucial for neutron slowing-down.

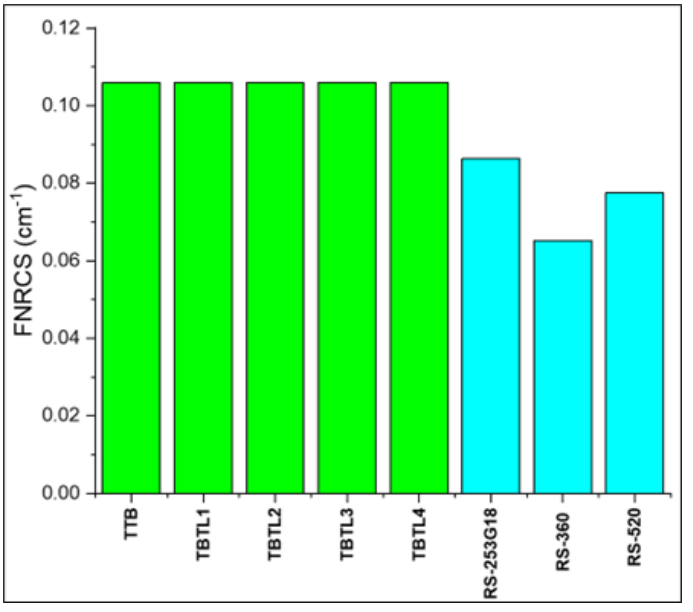


Fig. 5. Calculated fast neutron removal cross-section (Σ_R) values for the prepared TBTL glasses and selected commercial radiation shielding materials.

4. CONCLUSION

This study systematically evaluated the radiation shielding performance of a series of tellurite-based glasses with the composition $65TeO_2–25Bi_2O_3–(10\text{-}x)TiO_2–xLa_2O_3$, where x varied from 1 to 4. Using the Phy-X/PSD simulation platform, key shielding parameters were examined across an extensive energy range from 0.015 to 15 MeV. The findings reveal a consistent improvement in shielding effectiveness with increasing La_2O_3 concentration, which corresponds directly to a rise in the density of the glass samples. Among the tested compositions, the sample with the highest La_2O_3 content exhibited the most favorable shielding characteristics, including lower half-value layers and mean free paths, indicating a greater capacity to attenuate ionizing radiation. Comparative analysis with commercially available shielding materials such as RS-253 G18, RS-360, and RS-520 demonstrated that the fabricated tellurite glasses provide superior attenuation, particularly at higher photon energies. Additionally, the fast neutron removal cross-section values of the developed glasses were found to be competitive with existing standard materials, although they showed relatively lower neutron hardening performance. The enhanced shielding capability is attributed to the increased effective atomic number and electron density imparted by the incorporation of rare earth oxides, which promote greater interaction with incident radiation through photoelectric absorption, Compton scattering, and pair production processes. These results underscore the potential of rare earth-doped tellurite glasses as effective, non-toxic alternatives to conventional lead-based shielding materials. Given their promising radiation attenuation properties, these glasses are well-suited for applications in diverse environments such as medical radiotherapy facilities, nuclear research institutions, airport security installations, and industrial radiography setups. Future work may focus on optimizing the compositional ratios, scaling up production, and assessing long-term stability and environmental impact to facilitate practical deployment.

DECLARATIONS

Ethical Approval

We affirm that this manuscript is an original work, has not been previously published, and is not currently under consideration for publication in any other journal or conference proceedings. All authors have reviewed and approved the manuscript, and the order of authorship has been mutually agreed upon.

Funding

Not applicable

Availability of data and material

The datasets used and/or analyzed during the current study are available from the corresponding author on reasonable request.

Conflicts of Interest

The authors declare that they have no financial or personal

© Ariston Publications 2025. All rights reserved.

interests that could have influenced the research and findings presented in this paper. The authors alone are responsible for the content and writing of this article.

Authors' contributions

Zahrah S.A Almutawah: Conceptualization, Methodology, Investigation, Writing—original draft, Formal analysis, Writing—review and editing, , Funding acquisition; Ibrahim Hadadi: Methodology, Writing—review and editing, Visualization; Awad Almarhaby: Conceptualization, Methodology, Formal anal-ysis, Investigation, Writing—original draft; Ibtesam S. Asiri: Methodology, Writ-ing—review and editing, Visualization; Elhussaien Elshiekh: Formal analysis, Investigation, Visualization; Badriah Sultan: Conceptualization, Methodology, Investigation, Writing—review and editing, Visualization.

ACKNOWLEDGEMENTS

The authors extend their appreciation to the Ministry of Education in KSA for funding this research work through the project number KKU- IFP2-DA-6.

REFERENCES

[1] Alqahtani, M.S., Almarhaby, A.M., Hussein, K.I., AbouDeif, Y.M., Afifi, H., Zahran, H., Yaha, I.S., Grelowska, I. and Yousef, E., **2021.** Radiation attenuation and photoluminescence properties of host tellurite glasses doped with Er3+ ions. *Journal of Instrumentation*, *16*(01), p.P01002.

[2] El-Denglawey, A., Zakaly, H.M., Alshammari, K., Issa, S.A., Tekin, H.O., AbuShanab, W.S. and Saddeek, Y.B., **2021.** Prediction of mechanical and radiation parameters of glasses with high Bi_2O_3 concentration. *Results in Physics*, *21*, p.103839.

[3] Susoy, G., **2020.** Effect of TeO_2 additions on nuclear radiation shielding behavior of $Li_2O–B_2O_3–P_2O_5–TeO_2$ glass-system. *Ceramics International*, *46*(3), pp.3844-3854.

[4] Alzahrani, J.S., Sriwunkum, C., Tonguc, B.T., Alothman, M.A., Olarinoye, I.O. and Al-Buriahi, M.S., **2023.** Lead-free bismuth glass system towards eco-friendly radiation shielding applications. *Results in Physics*, *53*, p.106987.

[5] Ji, S., Huang, W., Guo, J., Wang, J., Lu, X., Huang, D., Wei, H., Fan, W. and Li, X., **2021.** Lamp-pumped eight-pass neodymium glass laser amplifier with high beam quality. *Optical and Quantum Electronics*, *53*(6), p.277.

[6] Elkhoshkhany, N. and Mohamed, H.M., **2019.** UV–Vis-NIR spectroscopy, structural and thermal properties of novel oxyhalide tellurite glasses with composition TeO_2-B_2O_3-$SrCl_2$-LiF-Bi_2O_3 for optical application. *Results in Physics*, *13*, p.102222.

[7] Elkhoshkhany, N. and Essam, R., **2020.** Influence of La_2O_3 on the structural, optical and thermal properties of $TeO_2–ZnO–Li_2O–Nb_2O_5$ glass. *Journal of Non-Crystalline Solids*, *536*, p.119994.

[8] Murugan, G.S., Fargin, E., Rodriguez, V., Adamietz, F., Couzi, M., Buffeteau, T. and Le Coustumer, P., **2004.** Temperature-assisted electrical poling of $TeO_2–Bi_2O_3–ZnO$ glasses for non-linear optical applications. *Journal of Non-Crystalline Solids*, *344*(3), pp.158-166.

[9] Al-Hadeethi, Y., Sayyed, M.I., Mohammed, H. and Rimondini, L., **2020.** X-ray photons attenuation characteristics for two tellurite based glass systems at dental diagnostic energies. *Ceramics International*, *46*(1), pp.251-257.

[10] El-Mallawany, R., **1992.** The optical properties of tellurite glasses. *Journal of Applied Physics*, *72*(5), pp.1774-1777.

[11] Al-Buriahi, M.S. and Rammah, Y.S., **2019.** Electronic polarizability, dielectric, and gamma-ray shielding properties of some tellurite-based glasses. *Applied Physics A*, *125*(10), p.678.

[12] Al-Buriahi, M.S. and Mann, K.S., **2019.** Radiation shielding investigations for selected tellurite-based glasses belonging to the TNW system. *Materials Research Express*, *6*(10), p.105206.

[13] Alqahtani, F.F., Alzuhair, A.Z., Mohamed, S.E., Zahran, H.Y., Alqahtani, M.S., Hussein, K.I., Alshehri, A.M., Yahia, I.S., Reben, M. and Yousef, E.S., **2022.** Correlation of physical parameters features with optical and radiation shielding properties of heavy glass. *Radiation Physics and Chemistry*, *196*, p.110098.

[14] Hussein, K.I., Alqahtani, M.S., Alzahrani, K.J., Alqahtani, F.F., Zahran, H.Y., Alshehri, A.M., Yahia, I.S., Reben, M. and Yousef, E.S., **2022.** The effect of ZnO, MgO, TiO_2, and Na_2O modifiers on the physical, optical, and radiation shielding properties of a TeTaNb glass system. *Materials*, *15*(5), p.1844.

[15] Alqahtani, F.F., Alzuhair, A.Z., Mohamed, S.E., Zahran, H.Y., Alqahtani, M.S., Hussein, K.I., Alshehri, A.M., Yahia, I.S., Reben, M. and Yousef, E.S., **2022.** Correlation of physical parameters features with optical

 © Ariston Publications 2025. All rights reserved.

and radiation shielding properties of heavy glass. *Radiation Physics and Chemistry*, *196*, p.110098.

[16] Kim, S.H., Yoko, T. and Sakka, S., **1993.** Linear and nonlinear optical properties of TeO_2 glass. *Journal of the American Ceramic Society*, *76*(10), pp.2486-2490.

[17] Çağlar, İ., Cengiz, G.B. and Bilir, G., **2021.** Gamma radiation shielding properties of some binary tellurite glasses. *Journal of Non-Crystalline Solids*, *574*, p.121139.

[18] Udovic, M., Thomas, P., Mirgorodsky, A., Durand, O., Soulis, M., Masson, O., Merle-Méjean, T. and Champarnaud-Mesjard, J.C., **2006.** Thermal characteristics, Raman spectra and structural properties of new tellurite glasses within the Bi_2O_3–TiO_2–TeO_2 system. *Journal of Solid State Chemistry*, *179*(10), pp.3252-3259.

[19] Halimah, M.K., Azuraida, A., Ishak, M. and Hasnimulyati, L., **2019.** Influence of bismuth oxide on gamma radiation shielding properties of boro-tellurite glass. *Journal of Non-Crystalline Solids*, *512*, pp.140-147.

[20] Albarzan, B., Hanfi, M.Y., Almuqrin, A.H., Sayyed, M.I., Alsafi, H.M. and Mahmoud, K.A., **2021.** The influence of titanium dioxide on silicate-based glasses: an evaluation of the mechanical and radiation shielding properties. *Materials*, *14*(12), p.3414.

[21] Elkhoshkhany, N., Marzouk, S., El-Sherbiny, M., Ibrahim, H., Burtan-Gwizdala, B., Alqahtani, M.S., Hussien, K.I., Reben, M. and Yousef, E.S., **2022.** Investigation of structural, physical, and attenuation parameters of glass: TeO_2-Bi_2O_3-B_2O_3-TiO_2-RE_2O_3 (RE: La, Ce, Sm, Er, and Yb), and applications thereof. *Materials*, *15*(15), p.5393.

[22] Hussein, K.I., Alqahtani, M.S., Alzahrani, K.J., Zahran, H.Y., Alshehri, A.M., Yahia, I.S., Reben, M. and Yousef, E.S., **2022.** The Investigation of New Phosphate–Titanite Glasses According to Optical, Physical, and Shielding Properties. *Crystals*, *12*(7), p.941.

[23] Şakar, E., Özpolat, Ö.F., Alım, B., Sayyed, M.I. and Kurudirek, M., **2020.** Phy-X/PSD: development of a user friendly online software for calculation of parameters relevant to radiation shielding and dosimetry. *Radiation Physics and Chemistry*, *166*, p.108496.

[24] Hubbell, J.H., **1999.** Review of photon interaction cross section data in the medical and biological context. *Physics in Medicine & Biology*, *44*(1), p.R1.

[25] Tekin, H.O., Kavaz, E., Papachristodoulou, A., Kamislioglu, M., Agar, O., Guclu, E.A., Kilicoglu, O. and Sayyed, M.I., **2019.** Characterization of SiO_2–PbO–CdO–Ga_2O_3 glasses for comprehensive nuclear shielding performance: Alpha, proton, gamma, neutron radiation. *Ceramics International*, *45*(15), pp.19206-19222.

[26] Komatsu, T. and Dimitrov, V., **2020.** Features of electronic polarizability and approach to unique properties in tellurite glasses. *International Journal of Applied Glass Science*, *11*(2), pp.253-271.

[27] Şakar, E., Özpolat, Ö.F., Alım, B., Sayyed, M.I. and Kurudirek, M., **2020.** Phy-X/PSD: development of a user friendly online software for calculation of parameters relevant to radiation shielding and dosimetry. *Radiation Physics and Chemistry*, *166*, p.108496.

[28] El-Agawany, F.I., Tashlykov, O.L., Mahmoud, K.A. and Rammah, Y.S., **2020.** The radiation-shielding properties of ternary SiO_2–SnO–SnF_2 glasses: simulation and theoretical study. *Ceramics International*, *46*(15), pp.23369-23378.

[29] Hanfi, M.Y., Sayyed, M.I., Lacomme, E., Akkurt, I. and Mahmoud, K.A**., 2021.** The influence of MgO on the radiation protection and mechanical properties of tellurite glasses. *Nuclear Engineering and Technology*, *53*(6), pp.2000-2010.

[30] Kurtulus, R., Kurtulus, C. and Kavas, T., **2021.** Physical, optical, thermal, mechanical, and photon shielding properties of Rb_2O-reinforced SiO_2–Na_2O–CaO–MgO–Al_2O_3 glass system. *Journal of Materials Science: Materials in Electronics*, *32*(6), pp.7801-7814.

© Ariston Publications 2025. All rights reserved.